NANO · MICRO
small
www.small-journal.com

Modulating the Surface State of SiC to Control Carrier Transport in Graphene/SiC

Yuping Jia, Xiaojuan Sun, Zhiming Shi, Ke Jiang, Henan Liu, Jianwei Ben, and Dabing Li**

Silicon carbide (SiC) with epitaxial graphene (EG/SiC) shows a great potential in the applications of electronic and photoelectric devices. The performance of devices is primarily dependent on the interfacial heterojunction between graphene and SiC. Here, the band structure of the EG/SiC heterojunction is experimentally investigated by Kelvin probe force microscopy. The dependence of the barrier height at the EG/SiC heterojunction to the initial surface state of SiC is revealed. Both the barrier height and band bending tendency of the heterojunction can be modulated by controlling the surface state of SiC, leading to the tuned carrier transport behavior at the EG/SiC interface. The barrier height at the EG/SiC(000-1) interface is almost ten times that of the EG/SiC(0001) interface. As a result, the amount of carrier transport at the EG/SiC(000-1) interface is about ten times that of the EG/SiC(0001) interface. These results offer insights into the carrier transport behavior at the EG/SiC heterojunction by controlling the initial surface state of SiC, and this strategy can be extended in all devices with graphene as the top layer.

1. Introduction

Recently, there are tremendous quests for applying wafer-size silicon carbide (SiC) covered with epitaxial graphene (EG) in radio frequency (RF) and photodetector (PD) devices.[1–7] In these devices, the properties both of graphene and SiC are combined together to get high performance.[8–12] Even though the optimized growth process[13,14] and integrated technology[2,14] have been tried, the performance of EG/SiC devices is still far from the expectation. The EG/SiC interface has been paid more and more attention and considered to play the key role to the performance of the devices. In RF devices, the interfacial state at EG/SiC(0001) has a negative impact on the carrier mobility in graphene.[15] However in PDs, the interfacial heterojunction makes the photogenerated carriers transport across the interface easily, which minimizes the recombination losses.[5] In addition, a high photogenerated carrier injection efficiency can be achieved as the result of the especial carrier transport behavior across the EG/SiC junction at interface.[7] Thus, controlling the interfacial states is very important to obtain high performance PDs.

There are two ways to modulate the interfacial atomic state. One is adjusting the interfacial atoms by external force after graphene growth, such as intercalation.[16–19] Unfortunately, it is not easy to realize. The other is controlling the surface of substrate before graphene growth to modulate the interfacial state. As well known, the different terminal surfaces always result in different interfacial atomic stacking. For SiC(0001), the buffer layer exists at interface between graphene and SiC. It has a $(6\sqrt{3}\times 6\sqrt{3})R30$ periodicity with a mixture of sp^2 and sp^3 bonding. For SiC(000-1), there may be (2 × 2) stacking at the interface of EG/SiC(000-1).[20,21] For these interfacial atomic stackings, the different forms of energy band bending exist, which will lead to different types of junctions. However, the dependence of interfacial band structure to the initial surface state of SiC has not been studied in detail.

Here, the interfacial states between graphene and SiC substrate are investigated. The surface sensitive spectroscopy of Kelvin probe force microscopy (KPFM)[22–24] is used to measure the surface potential both in dark condition and under UV illumination. The behavior of photogenerated carrier transport can be obtained. Furthermore, the dominant factor to control the interfacial band structure is demonstrated as the initial surface state of SiC. The almost ten times amount of photogenerated carriers transfer from SiC(000-1) to graphene compared with that for EG/SiC(0001) system has been observed. The high carrier injection efficiency can be achieved using EG/SiC(000-1). The results here identify a new way to modulate the interfacial heterojunction in EG/SiC devices by controlling the initial surface state of SiC substrate.

2. Results and Discussion

To identify the photogenerated carrier transport between SiC and graphene, the discrete graphene is prepared. Here, growth

---

Dr. Y. P. Jia, Prof. X. J. Sun, Prof. Z. M. Shi, Dr. K. Jiang,
H. N. Liu, Dr. J. W. Ben, Prof. D. B. Li
State Key Laboratory of Luminescence and Applications
Changchun Institute of Optics
Fine Mechanics and Physics
Chinese Academy of Sciences
Changchun 130033, P. R. China
E-mail: sunxj@ciomp.ac.cn; lidb@ciomp.ac.cn

Dr. K. Jiang, Dr. J. W. Ben
University of Chinese Academy of Sciences
Beijing 100039, P. R. China

The ORCID identification number(s) for the author(s) of this article can be found under https://doi.org/10.1002/smll.201801273.

DOI: 10.1002/smll.201801273

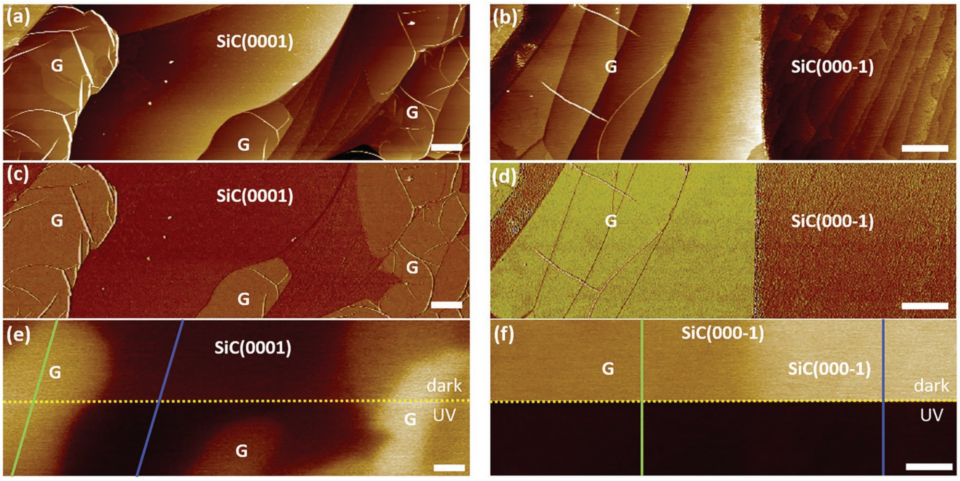

Figure 1. a,b) The morphology images of graphene partially grown on Sample A and Sample B are shown. c,d) Corresponding to the morphology images, the phase images of insets (a) and (b) are shown. The different contrast in phase images means there are two parts of the sample. One is the area with graphene which has the bright contrast and the other is the area without graphene which has the dark contrast. Both of these two regions are marked here, and the "G" for graphene and "SiC(0001)/SiC(000-1)" for bare SiC(0001)/(000-1) surface. e,f) The surface potential images in dark (the upper part) condition and under UV illumination (bottom part) are shown. The yellow lines are the boundaries of these two parts. And the surface potential profiles along the green and blue lines are shown in Figure S2 in the Supporting Information. All the scale bars here are 1 µm.

time and growth temperature are adjusted to obtain partial growth graphene on SiC(0001) substrate successfully. However, due to high growth rate of graphene on SiC(000-1) substrate, the discrete graphene cannot be obtained by adjusting growth parameters. Thus a SiC cover is placed on one half part of SiC(000-1) substrate to prevent Si atoms escaping from the surface. Meanwhile, another half part of SiC is exposed to the atmosphere for growth of graphene. At the boundary of these two parts, the noncontinuous graphene has been achieved. The morphology of discrete graphene on SiC(0001) (Sample A) and SiC(000-1) (Sample B) are clearly seen (**Figure 1**a,b). A very good correlation between the phase images[25] (Figure 1c,d) with the morphology images can be found. The wrinkles (the white lines) exist in the graphene regions, where the bright contrast in phase images can be observed. The Raman spectra of Samples A and B are used to determine the quality and layer number of graphene (Figure S1, Supporting Information). The neglected D peak and high intensity single Lorentz 2D peak determine that the EG/SiC(000-1) and EG/SiC(0001) are mono- and bilayer high-quality graphene.[26,27] The KPFM characterization is utilized to measure the surface potential (Figure 1e,f). The upper and bottom parts are taken in dark and under UV illumination, respectively. When UV light projects on the EG/SiC(0001), the small diminution of surface potential in the graphene region and the graphene-free region can be more clearly illustrated by surface potential profile curves (Figure S2, Supporting Information) along the green and blue lines. On the contrary, the surface potential of EG/SiC(000-1) shows significant decrease under UV illumination obviously (Figure 1f; Figure S2b, Supporting Information). The change of the surface potential is attributed to the photogenerated carrier transport between SiC and graphene. In order to obtain the accurate value of surface potential change, the KPFM measurements have been taken in the bottom region both in dark and under UV illumination (**Figure 2**). The surface potential profile curves are extracted along the orange and red lines at the same position. For both Samples A and B, the values of surface potential decrease under UV illumination. In the case of EG/SiC(0001), the diminution of the surface potential is about 50 mV in region III of bare SiC substrate (Figure 2e). In region I with graphene on the surface, the surface potential decreases with the value of 45 mV which is close to the value of region III. The diminution value of the region II with graphene is 20 mV. It is smaller than that of region III. In the case of EG/SiC(000-1), the diminution of the surface potential in left region with graphene is 238 mV (Figure 2f). The diminution of the surface potential in right region without graphene is 310 mV, which is a little larger than that of graphene. The variation of energy band of graphene and SiC surface dominated by the photogenerated carriers is the reason for the surface potential change as KPFM measured.

To ensure the photogenerated carrier transport behavior, the band structure is plotted here according to the KPFM results. The carrier type of graphene needs to be identified using the electrically biased tapping mode (eb-TM) method.[28,29] As the eb-TM measured, the height of graphene and bare SiC are observed under different tip bias (Figure S3, Supporting Information). The height of graphene is changed as the result of the carrier accumulation at the surface drove by tip bias. If the major carrier is electron, the amount of electrons accumulated under positive bias is more than the amount of holes accumulated under negative bias. As a result, the height of graphene under positive bias is higher than that under negative bias. Therefore, the graphene in the region I is n-type (**Figure 3**a–c). It is different for the case of EG/SiC(0001) in the region II (Figure 3d–f). At ±4 V bias, the height of graphene under positive bias is higher than that under negative bias. Thus the initial carrier type of graphene is n-type. When the voltage increases to ±6 and ±8 V, the height of graphene under negative bias is higher than that under positive bias. This inversion means the carrier type of graphene under the bias ±6 and ±8 V is changed from n-type into p-type. As calculation, the external

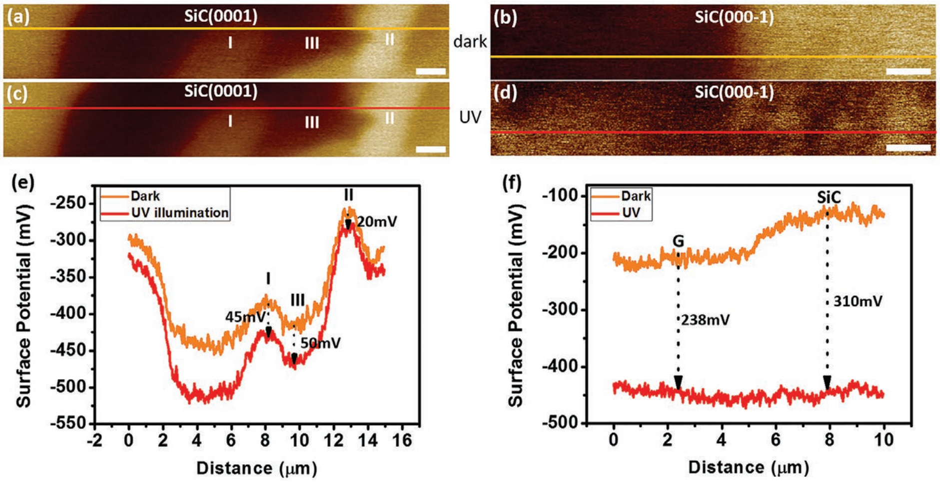

Figure 2. a,b) The surface potential images of graphene partially grown on Sample A and Sample B in the dark condition are shown. c,d) And the surface potential images of the same region in UV condition are shown correspondingly. e) The surface potential along the orange and red lines in insets (a) and (c) are shown. The value of the potential change in region I, II, and III are shown in inset (e) respectively. f) The surface potential along the orange and red lines in insets (b) and (d) are shown. And the left region is with graphene and the right region is without graphene. The value of the potential change for these two regions is given in inset (f). All the scale bars in insets (a)–(d) are 1 μm.

bias can accumulate the charge on the top layer of graphene,[30] which has significant influence on the carrier type of graphene. Though the amount of charges accumulated from substrate is neglectable in the case of SiC(0001), the holes should come from the adsorbed molecules such as water and oxygen molecules in the air. As the water and oxygen molecules always act

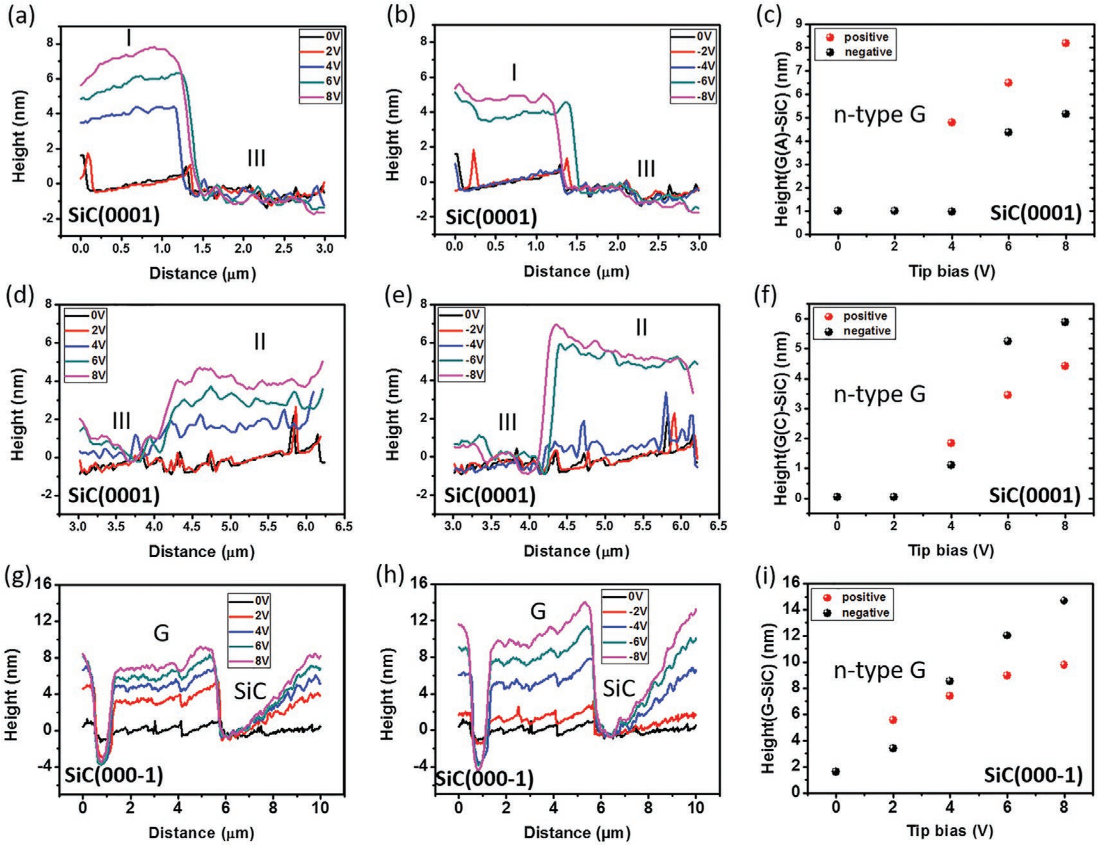

Figure 3. The eb-TM is used here to identify the carrier type of graphene. a,b) In the case of EG/SiC(0001) (Sample A), the height for graphene in region I at different bias voltage are shown. c) The height difference between graphene and SiC in region I is collected. d,e) And the height profiles for graphene in region II are shown. f) The height difference between graphene and SiC in region II is collected. g–i) In the condition of EG/SiC(000-1) (Sample B), the same characterization by eb-TM are taken and the results are shown.

as acceptor, the holes easily transfer to graphene.[31,32] On the contrary, there are small amount of electrons transfer from water and oxygen molecules to graphene even under large positive bias. The amount of holes accumulated on graphene under large negative bias is much more than that of electrons accumulated under positive bias. So it is shown as p-type, which is consistent with KPFM results. The holes accumulation on graphene under negative bias also happens in case of region I. However, there might be large initial electron density of graphene in region I, which makes the inversion of carrier type not achieve. For EG/SiC(000-1) system, the change from n-type (±2) to p-type (≥ ± 4 V) is also observed (Figure 3g–i). In the case of EG/SiC(000-1), holes accumulate both from substrate and adsorbed molecules under negative bias. Thus the carrier type can change from n-type into p-type at small bias.

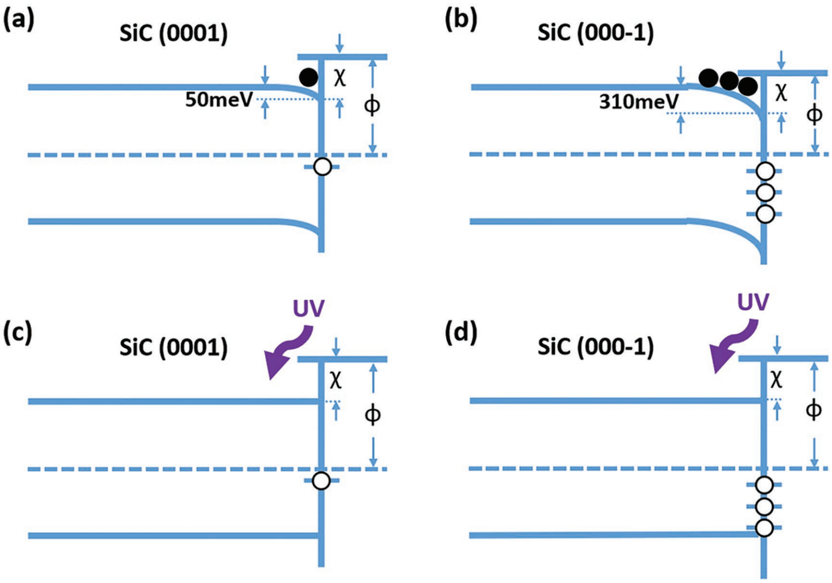

Figure 4. a) The band diagram of SiC (0001) (Sample A) is shown. b) The band diagram of SiC (000-1) (Sample B) is shown. According to the results of KPFM, both of them have empty surface donor states which accumulate electrons at the surface. The downward band bending can be deduced as the result of the electron accumulation. And the value of band bending for SiC(0001) and SiC(000-1) are 50 and 310 meV respectively. c,d) Under UV illumination, the bending band will recover to flat as shown.

The band structure has been plotted using the results of surface potential and carrier type measurement. First, the band structure of bare SiC(0001) and SiC(000-1) are described (**Figure 4**). According to the KPFM results, the decrease of surface potential for both SiC(0001) and SiC(000-1) under UV light indicates the increase of work function for SiC surface according to the Equation (1).[33,34] The downward band bending at the surface of SiC can be deduced. Under UV illumination, the band will become flat and the work function will increase

$$V_{\mathrm{CPD}} = V_{\mathrm{sample}} - V_{\mathrm{tip}} = \frac{\phi_{\mathrm{tip}} - \phi_{\mathrm{sample}}}{e} \tag{1}$$

As well know, the accumulation of electrons due to the empty donor surface state may results downward band bending.[35] When under UV illumination, the photogenerated holes will transfer from bulk SiC to surface. Simultaneously electrons accumulated at surface will transfer to the bulk SiC and the band bending will recovered. As a result, the work function increases, which agrees with the results of KPFM. Therefore, the existence of empty donor surface state can be proved. When graphene grown on SiC, the electron will transfer from donor at SiC surface to graphene, which cause the built-in field at EG/SiC interface and thus the upward bending of the band structure at interface (**Figure 5**). Under UV illumination, the photogenerated holes transfer from SiC to graphene which is driven by the built-in field. The Fermi level of graphene will go down and the work function of graphene will become larger which indicates the decrease of the surface potential for graphene. It is consistent with the results of KPFM. The diminutions of the surface potential are about 45, 20, and 238 meV for graphene on SiC(0001) in region I, graphene on SiC(0001) in region II, and graphene on SiC(000-1), respectively. According to these results, the value of upward band bending at the interface is 45 meV (or 20 meV) for graphene on SiC(0001) in region I, which is at the same order of magnitude for the value of

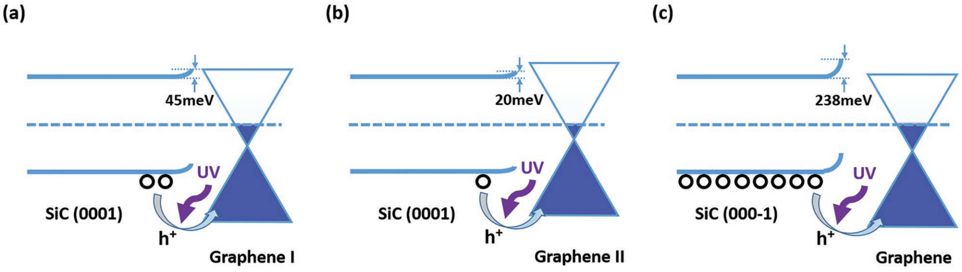

Figure 5. The band diagram of EG/SiC system of Sample A and B are shown here. a) The band diagram of EG/SiC(0001) in region I. The upward bending at interface and n-type graphene are given. Under UV illumination, holes transfer from SiC to graphene. b) The band diagram of EG/SiC(0001) in region II. The upward bending at interface and n-type graphene are also given. The value of band bending is 20 meV smaller than 45 meV for EG/SiC(0001) in region I. Under UV illumination, holes transfer from SiC to graphene and the amount of holes is smaller than EG/SiC(0001) in region I. c) In the case of EG/SiC(000-1), the value of upward band bending is 238 meV as shown. The amount of holes transferring from SiC to graphene is the largest in all three cases.

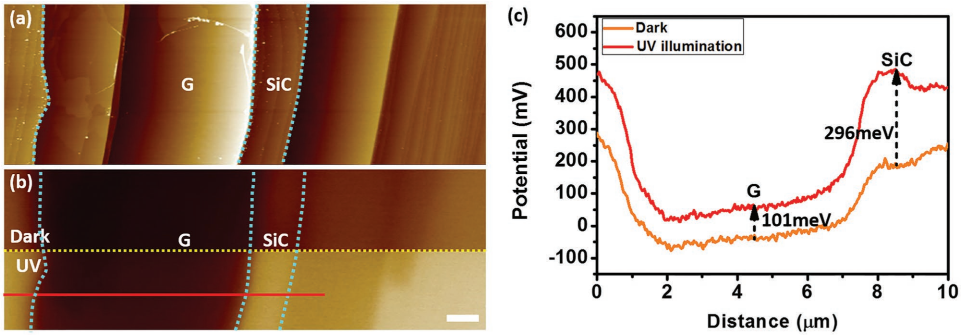

Figure 6. a) The surface morphology of Sample C is given. The region with graphene has big steps and the region without graphene has small steps. The blue dot lines are marked the boundary of these two regions. b) The surface potential at the same region of inset (a) is shown. The upper part is taken in dark condition and the bottom part is taken under UV illumination. The yellow line is the boundary line. c) Along the red line, the surface potential profiles in dark condition and UV condition are collected. The values of potential increase for graphene and bare SiC are given. The scale bar here is 1 μm.

downward band bending for bare SiC (about 50 mV). It means the built-in field at interface which induces the band bending is dominated by the surface donor state of SiC. However, both in region I and region II with graphene, the smaller band bending are observed than that in region III of bare SiC. The electrons transfer not only from interface into graphene, but also from interface to bulk SiC. This might be the reason why the upward band bending at interface is smaller than the downward bending at initial SiC surface. In the case of EG/SiC(000-1), the same behavior has been observed. The upward band bending of 238 meV is near to 310 meV for bare SiC(000-1). It is about ten times of EG/SiC(0001). All these results come to a conclusion that the surface donor state of SiC is the key factor for the upward band bending at the EG/SiC interface. And the large band bending of initial SiC surface state will lead to a large band bending at the interface in EG/SiC system. The amount of carriers transferring from SiC to graphene under UV illumination depends on the barrier height of the junction, which is the result of the band bending at interface. Thus the modulation of initial surface state can be used to control the amount of carriers injecting into graphene from SiC.

On the other hand, if the surface states of SiC are filled acceptors, the downward band bending at EG/SiC interface and the transport of electrons from SiC to graphene under UV illumination can be expected. It is proved by another EG/SiC(000-1) sample (Sample C). The graphene is grown only in the region with big-step morphology on SiC(000-1) (**Figure 6**a). The graphene with big-step morphology and the bare SiC substrate with small-step morphology can be observed. As characterization of eb-TM (Figure S4, Supporting Information), the graphene on Sample C is n-type. The comparison between the potential in dark condition and under UV illumination is given (Figure 6b). The increase of the potential can be observed obviously when UV light projects on the Sample C. This result is opposite to Samples A and B. The amplitude of increase in the region of bare SiC is about 296 mV and it is 101 mV for the region with graphene (Figure 6c). The full filled acceptor surface states can be deduced. The holes are accumulated at the surface of SiC, which results in the upward band bending (**Figure 7**a). When UV light projects on SiC, the photogenerated electrons transfer from bulk SiC to the surface. Therefore, the band structure of surface becomes flat (Figure 7b). The work function of SiC surface decreases and the surface potential of SiC increases, which is correspondence with the KPFM results. The increased value of surface potential for bare SiC is 296 mV. As a result the value of upward band bending is 296 meV. In the region with graphene, the surface potential will also increase under UV illumination. Thus the downward band bending exists at the interface between SiC and graphene. The photogenerated electrons transferring from SiC to graphene is driven by the built-in field, which results in the increase of Fermi level. According to Equation (1), the surface potential of graphene increases. It agrees with KPFM results. The value of band bending at interface is about 101 meV (Figure 7c).

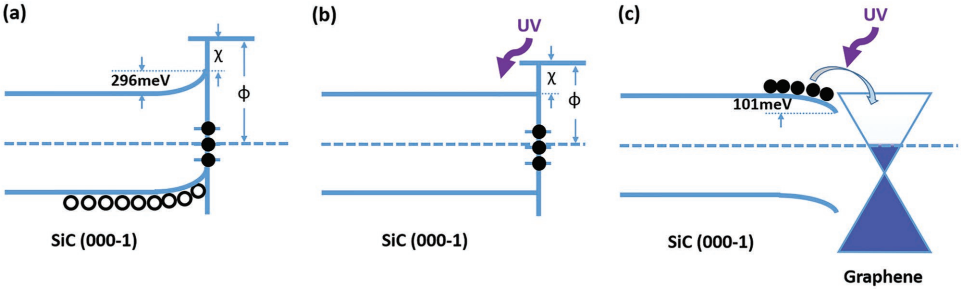

Figure 7. The band diagram of Sample C is shown here. a) The band diagram of SiC surface is shown. According to the results of KPFM, it has filled surface acceptor states which accumulate holes at the surface. The upward band bending can be deduced. And the value of band bending is 296 meV. b) Under UV illumination, the bending band recover to flat as shown. c) The band diagram of EG/SiC system are shown. The downward bending at interface and n-type graphene are given. Under UV illumination, electrons transfer from SiC to graphene.

These results ensure that the full filled acceptor surface state of SiC will lead to the downward band bending at the interface between SiC and graphene. It confirms that the surface state of SiC is the key factor for the interface band structure. The band bending tendency at interface depends on the type of SiC surface state. The value of band bending is always at the same order of magnitude as the surface band bending of SiC, which depends on the density of surface state. These results offer a new way to control interface band structure and to adjust the barrier height of heterojunction at interface. Basing on modulation of the heterojunction, the high-efficiency and low reverse leakage might be achieved in device. In addition, the interface built-in field at EG/SiC(000-1) system is always bigger than that at EG/SiC(0001) system. The largest barrier of heterojunction in EG/SiC(000-1) (Sample B) is ten times higher than that in EG/SiC(0001). Thus about ten times carrier has been observed to transfer from SiC(000-1) to graphene than that from SiC(0001) to graphene. It will lead to a higher carrier injection efficiency in EG/SiC(000-1) device. Combining with the high carrier mobility, high thermal conductivity and weak interaction between graphene and SiC(000-1) substrate, the better performance of device, even flexible device, based on EG/SiC(000-1) material is promising in the future.

3. Conclusion

As determined by KPFM, the photogenerated carrier transport behavior between graphene and SiC substrate is observed directly. Results reveal the dependence of heterojunction at EG/SiC interface to initial surface state of SiC. The surface donor state of SiC leads to an upward bending of band structure at interface, and surface acceptor state of SiC results a downward bending of band structure at interface. The amount of transport carrier is also demonstrated to depend on the initial surface state density of SiC. Thus the modulation of carrier transport can be achieved by controlling the initial surface state of SiC. Further, more surface donor state in SiC(000-1) is always observed than that in SiC(0001). As a result, the height of barrier in EG/SiC(000-1) system interface can be ten times higher than that in EG/SiC(0001) system, which leads to almost ten times amount of carrier transferring from SiC(000-1) to graphene compared with that from SiC(0001) to graphene. The high barrier junction in EG/SiC(000-1) will lead to a large injection and sensitivity in PD devices. It provides a new way to obtain a high performance PD devices using EG/SiC(000-1). The method presented here is a promising way to modulate the carrier transport behavior at EG/SiC interface.

4. Experimental Section

The epitaxial graphene was achieved through a thermal decomposition of commercially available semi-insulating SiC with (0001) surface (Sample A) and (000-1) surface (Samples B and C) polished respectively. To identify the photogenerated carrier transport between graphene and SiC, the discrete graphene was prepared. Thus the controllable process should be used to sublimate Si atoms to fabricate graphene on SiC substrate. For SiC(0001) surface, the growth rate of graphene was slow so that it can be easy to obtain partial growth graphene by decreasing the growth time and growth temperature. However, the growth rate of graphene on SiC (000-1) was very large and it was impossible to achieve discrete graphene by the foregoing way the same as EG/SiC(0001). For preparing the discrete graphene, one half part of SiC(000-1) substrate was covered with SiC wafer, and another half was exposed to the atmosphere for growth of graphene. At the boundary between these two parts, the noncontinuous graphene on SiC(000-1) was obtained successfully. The morphology of EG/SiC was given by the tapping mode of atomic force microscopy (AFM) (Bruker multimod8). And the layer number and quality of graphene were determined through Raman spectrum (Horiba LabRAM HR Evolution). To characterize the carrier property, the et-TM and KPFM as the electric mode of AFM (Bruker multimod8) were used.

Supporting Information

Supporting Information is available from the Wiley Online Library or from the author.

Acknowledgements

This work was supported by the National Key R&D Program of China (2016YFE0118400), National Science Fund for Distinguished Young Scholars (61725403), the National Natural Science Foundation of China (61574142, 61704171, 11705206), the Key Program of the International Partnership Program of CAS (181722KYSB20160015), the Science and Technology Service Network Initiative of the Chinese Academy of Sciences, the Jilin Provincial Science & Technology Department (20150519001JH, 20180201026GX), the CAS Interdisciplinary Innovation Team, the Youth Innovation Promotion Association of CAS (2015171), and the CAS Pioneer Hundred Talents Program.

Conflict of Interest

The authors declare no conflict of interest.

Keywords

carrier transport, graphene, KPFM, surface states

Received: April 3, 2018
Revised: April 20, 2018

---

[1] Y. M. Lin, C. Dimitrakopoulos, K. A. Jenkins, D. B. Farmer, H. Y. Chiu, A. Grill, P. Avouris, *Science* **2010**, *327*, 662.
[2] Z. Guo, R. Dong, P. S. Chakraborty, N. Lourenco, J. Palmer, Y. Hu, M. Ruan, J. Hankinson, J. Kunc, J. D. Cressler, C. Berger, W. A. de Heer, *Nano Lett.* **2013**, *13*, 942.
[3] J. S. Moon, D. Curtis, M. Hu, D. Wong, C. McGuire, P. M. Campbell, G. Jernigan, J. L. Tedesco, B. VanMil, R. Myers-Ward, C. Eddy Jr., D. K. Gaskill, *IEEE Electron Device Lett.* **2009**, *30*, 650.
[4] P. Avouris, *Nano Lett.* **2010**, *10*, 4285.
[5] T. J. Anderson, K. D. Hobart, J. D. Greenlee, D. I. Shahin, A. D. Koehler, M. J. Tadjer, E. A. Imhoff, R. L. Myers-Ward, A. Christou, F. J. Kub, *Appl. Phys. Express* **2015**, *8*, 041301.
[6] E. Kusdemir, D. Özkendir, V. Fırat, C. Çelebi, *J. Phys. D: Appl. Phys.* **2015**, *48*, 095104.
[7] V. S. N. Chava, S. U. Omar, G. Brown, S. S. Shetu, J. Andrews, T. S. Sudarshan, M. V. S. Chandrashekhar, *Appl. Phys. Lett.* **2016**, *108*, 043502.

[8] C. Berger, Z. M. Song, X. B. Li, X. S. Wu, N. Brown, C. Naud, D. Mayou, T. B. Li, J. Hass, A. N. Marchenkov, E. H. Conrad, P. N. First, W. A. de Heer, *Science* **2006**, *312*, 1191.
[9] F. Bonaccorso, Z. Sun, T. Hasan, A. C. Ferrari, *Nat. Photonics* **2010**, *4*, 611.
[10] L. X. Zhu, F. Y. Liu, H. T. Lin, J. J. Hu, Z. F. Yu, X. R. Wang, S. H. Fan, *Light: Sci. Appl.* **2016**, *5*, e16052.
[11] H. Y. Chen, H. Liu, Z. M. Zhang, K. Hu, X. S. Fang, *Adv. Mater.* **2016**, *28*, 403.
[12] B. Sun, Y. Sun, C. X. Wang, *Small* **2018**, *14*, 1703391.
[13] C. Dimitrakopoulos, Y. M. Lin, A. Grill, D. B. Farmer, M. Freitag, Y. N. Sun, S. J. Han, Z. H. Chen, K. A. Jenkins, Y. Zhu, Z. H. Liu, T. J. McArdle, J. A. Ott, R. Wisnieff, P. Avouris, *J. Vac. Sci. Technol., B: Nanotechnol. Microelectron.: Mater., Process., Meas., Phenom.* **2010**, *28*, 985.
[14] J. Kedzierski, P. L. Hsu, P. Healey, P. W. Wyatt, C. L. Keast, M. Sprinkle, C. Berger, W. A. de Heer, *IEEE Trans. Electron Devices* **2008**, *55*, 2078.
[15] G. G. Jernigan, B. L. VanMil, J. L. Tedesco, J. G. Tischler, E. R. Glaser, A. Davidson III, P. M. Campbell, D. K. Gaskill, *Nano Lett.* **2009**, *9*, 2605.
[16] I. Deretzis, A. L. Magna, *Phys. Rev. B* **2011**, *84*, 235426.
[17] R. Mu, Q. Fu, L. Jin, L. Yu, G. Z. Fang, D. L. Tan, X. H. Bao, *Angew. Chem., Int. Ed.* **2012**, *51*, 4856.
[18] M. H. Oliveira Jr., T. Schumann, F. Fromm, R. Koch, M. Ostler, M. Ramsteiner, T. Seyller, J. Marcelo, J. Lopes, H. Riechert, *Carbon* **2013**, *52*, 83.
[19] Z. J. Wang, M. M. Wei, L. Jin, Y. X. Ning, L. Yu, Q. Fu, X. H. Bao, *Nano Res.* **2013**, *6*, 399.
[20] L. Magaud, F. Hiebel, F. Varchon, P. Mallet, J. Y. Veuillen, *Phys. Rev. B* **2009**, *79*, 161405(R).
[21] F. Hiebel, L. Magaud, P. Mallet, J. Y. Veuillen, *J. Phys. D: Appl. Phys.* **2012**, *45*, 154003.
[22] A. Lochthofen, W. Mertin, G. Bacher, L. Hoeppel, S. Bader, J. Off, B. Hahn, *Appl. Phys. Lett.* **2008**, *93*, 022107.
[23] G. Nowak, J. L. Weyher, A. Khachapuridze, I. Grzegory, *J. Cryst. Growth* **2012**, *353*, 68.
[24] J. D. Wei, S. F. Li, A. Atamuratov, H. H. Wehmann, A. Waag, *Appl. Phys. Lett.* **2010**, *97*, 172111.
[25] X. Z. Zhou, S. He, K. A. Brown, J. Mendez-Arroyo, F. Boey, C. A. Mirkin, *Nano Lett.* **2013**, *13*, 1616.
[26] J. Röhrl, M. Hundhausen, K. V. Emtsev, Th. Seyller, R. Graupner, L. Ley, *Appl. Phys. Lett.* **2008**, *92*, 201918.
[27] L. M. Malard, M. A. Pimenta, G. Dresselhaus, M. S. Dresselhaus, *Phys. Rep.* **2009**, *473*, 51.
[28] L. L. Jiang, B. Wu, H. T. Liu, Y. Huang, J. Y. Chen, D. C. Geng, H. J. Gao, Y. Q. Liu, *Adv. Mater.* **2013**, *25*, 7015.
[29] Y. P. Jia, L. W. Guo, Z. L. Li, J. Huang, W. Lu, H. X. Chen, X. L. Chen, *Adv. Electron. Mater.* **2016**, *2*, 1500255.
[30] Y. F. Guo, W. L. Guo, C. F. Chen, *Phys. Rev. B* **2009**, *80*, 085424.
[31] O. Leenaerts, B. Partoens, F. M. Peeters, *Phys. Rev. B* **2008**, *77*, 125416.
[32] A. Piazza, F. Giannazzo, G. Buscarino, G. Fisichella, A. La Magna, F. Roccaforte, M. Cannas, F. M. Gelardi, S. Agnello, *Phys. Status Solidi A* **2016**, *213*, 2341.
[33] D. B. Li, X. J. Sun, Y. P. Jia, M. I. Stockman, H. P. Paudel, H. Song, H. Jiang, Z. M. Li, *Light: Sci. Appl.* **2017**, *6*, e17038.
[34] F. Yan, G. Chen, L. Lu, J. E. Spanier, *ACS Nano* **2012**, *6*, 2353.
[35] A. Soudi, C. H. Hsu, Y. Gu, *Nano Lett.* **2012**, *12*, 5111.